Geoderma 355 (2019) 113901

Contents lists available at ScienceDirect

Geoderma

journal homepage: www.elsevier.com/locate/geoderma

Soil microaggregate size composition and organic matter distribution as affected by clay content

Steffen A. Schweizer[a,*], Franziska B. Bucka[a], Markus Graf-Rosenfellner[b], Ingrid Kögel-Knabner[a,c]

[a] Soil Science, Weihenstephan Department of Ecology and Ecosystem Management, TUM School of Life Sciences Weihenstephan, Technical University of Munich, Emil-Ramann-Str. 2, 85354 Freising-Weihenstephan, Germany
[b] Soil Ecology, Institute of Forest Sciences, Faculty of Environment and Natural Resources, University of Freiburg, Bertoldstr. 17, 79098 Freiburg, Germany
[c] Institute for Advanced Study, Technical University of Munich, Lichtenbergstraße 2a, 85748 Garching, Germany

ARTICLE INFO

Handling Editor: Naoise Nunan

Keywords:
Soil aggregation
Aggregate size distributions
Soil texture
Organo-mineral associations
Dynamic image analysis

ABSTRACT

Aggregation assembles different size mixtures of soil particles into a larger architecture. Such mixtures impede resolving which particles build aggregates and how these control the accumulation of soil organic matter (OM). Here we present an approach to differentiate the size distributions of soil fractions in the size range of microaggregates (< 250 µm) from their dispersible particle-size distribution using dynamic image analysis. This approach enabled us to differentiate the magnitude and preferential size ranges of aggregates and non-aggregated particles. Wet sieving was used to isolate free microaggregate-sized fractions. Larger soil structures > 250 µm were sonicated to isolate occluded size fractions < 250 µm. To investigate the impact of soil texture, we analyzed topsoil samples of an arable site on Cambisol soils with a gradient in clay content of 16–37% and organic carbon concentrations of 10–15 g kg^{-1}. Our results demonstrate how soil texture governs aggregate size distributions: most water-stable microaggregates were found to be of approximately 30 µm diameter, independent of the clay content gradient. High-clay soils contain more water-stable macroaggregates (> 250 µm) and larger microaggregates in the 50–180 µm size range. The low-clay soils, on the other hand, contained more non-aggregated sand-sized particles > 100 µm which probably hampered the buildup of larger aggregates. The size distribution of particles < 100 µm in size fractions < 250 µm showed a similar prevailing soil texture pattern, with approximately 24% clay, 59% silt, and 17% sand-sized particles at all clay contents. In contrast to the prevailing texture pattern along the clay content gradient, 4% more clay-sized particles helped build up water-stable macroaggregates. In the low-clay soils, the aggregates were smaller and the size fractions < 53 µm had higher OM concentrations. This indicates that the low-clay soils held most of their OM in smaller microaggregates. Such arrangement of OM in smaller microaggregates demonstrates that soil texture may control OM stabilization mostly indirectly via the distribution of OM in different aggregate fractions. The occlusion of microaggregates in larger structures led to lower alkyl:O/N-alkyl ratios in ^{13}C nuclear magnetic resonance (NMR) spectroscopy, indicating increased preservation.

1. Introduction

Mineral soil particles are considered to control the storage of organic matter (OM) in soils (Baldock and Skjemstad, 2000; Christensen, 1992; Torn et al., 1997). This control is believed to be affected by the particle-size distribution of primary particles, or soil texture, which affect the surface adsorption and formation of organo–mineral associations (Baldock and Skjemstad, 2000; von Lützow et al., 2007; Wagner et al., 2007). The aggregation of these soil components into larger structural units can exert major control on OM stabilization through its occlusion and protection from decomposition (Oades, 1993; Totsche et al., 2018; Wiesmeier et al., 2019). Within larger macroaggregates occluded microaggregates (< 250 µm) can be formed (Angers et al., 1997; Oades, 1984; Six et al., 2002b). Microaggregates have been shown to stabilize OM over decadal-to-centennial timescales (Jastrow et al., 1996; Puget et al., 2000; Virto et al., 2010). The separation of free and occluded microaggregates is a suitable approach for better understanding how soil particles are arranged in smaller and larger aggregate structures. Resolving this arrangement will elucidate whether individual particles or their combinations into aggregates

* Corresponding author.
E-mail addresses: schweizer@wzw.tum.de (S.A. Schweizer), franziska.bucka@tum.de (F.B. Bucka), Markus.Graf-Rosenfellner@bodenkunde.uni-freiburg.de (M. Graf-Rosenfellner), koegel@wzw.tum.de (I. Kögel-Knabner).

https://doi.org/10.1016/j.geoderma.2019.113901
Received 27 March 2019; Received in revised form 1 August 2019; Accepted 3 August 2019

govern OM content.

Previous works have postulated the widely applied relationship that the content of clay-sized particles determines the OM content by increasing sorptive mineral surface area and by aggregate formation (Dexter et al., 2008; Oades, 1988). Many studies have used such an empirical relationship between clay content or its dispersibility and the soil OM content as a proxy for soil structure stabilization (Barré et al., 2017; Dexter et al., 2008; Graf-Rosenfellner et al., 2016; Jensen et al., 2019; Oades, 1988; Schjønning et al., 2012). Recent metastudies have concluded that clay content is limited as a proxy for OM stabilization while other chemical properties explain substantial parts of OM stabilization (Bailey et al., 2018; Rasmussen et al., 2018). A study using a C3/C4 vegetation chronosequence showed no clear relationship between phyllosilicate mineralogy and OM content in particle fractions (Fernández-Ugalde et al., 2016). To study the isolated effect of clay content, very few sites are available with a wide range of soil textures developed on similar parent material with comparable OM inputs (Schjønning et al., 2012). Here we took advantage of such a site with range clay content of 16–37% within the same agricultural plot under similar management.

Many studies on soil structure have focused on clay-sized particles and have not included silt or sand-sized particles as a potential component of soil aggregates. A simple subtraction has often been used to differentiate aggregates from primary particles that are presumably not included in the aggregates of a size fraction (Elliott et al., 1991; Kemper and Chepil, 1965; Six et al., 2002a). However, more recent publications have highlighted that sand grains may play an active role in aggregation through water menisci forces, leading to the coalescence of larger primary particles in aggregates (Ghezzehei and Or, 2000; Paradiś et al., 2017). In size fractions finer than sand, it is not feasible to account for unaggregated primary particles by simple subtraction. In the dispersion of soil structure with glass beads into sizes < 50 µm (Virto et al., 2008), a large portion of silt-sized particles were shown to be released from structural units > 50 µm, indicating that the arrangement of particles in larger-sized aggregate structures varies. An earlier study showed that various size fractions in the range of microaggregates contain clay and silt-sized building particles in varying proportions but at a similar ratio (Balabane and Plante, 2004). The arrangement of specific particle sizes into aggregate structures shapes the distribution of specific surface area (SSA), which is highest in fine particle fractions (Mayer and Xing, 2001; Pronk et al., 2011). Positive correlations of the fine particle content with total mineral-associated OC concentrations and OC concentrations in macroaggregates (Carter et al., 2003) demonstrated the essential relationship between fine particles and OM stabilization. The analysis of aggregate structures relies mostly on wet sieving, which separates soil into size fractions with wide size ranges. Such size fractions contain soil particles and aggregates. However, the proportion of aggregates, how many particles they combine, and how large these are remain unresolved in most studies. Soil aggregates in isolated size fractions need to be clearly distinguished from non-aggregated particles in the same fraction. Measurements of the aggregate sizes that result from the arrangement of particles into larger-sized aggregates add additional insights beside the mass contributions of size fractions. Automatic size analyses methods, such as dynamic image analysis, help resolve the microaggregate arrangement more precisely down to the resolution of several µm.

The occlusion of OM in microaggregates preserves both plant and microbial residues (Golchin et al., 1994; Totsche et al., 2018). Studies involving solid-state ^{13}C nuclear magnetic resonance (NMR) spectroscopy of density fractions have shown that occluded particulate OM fractions contain more O/N-alkyl C than non-occluded ones (Golchin et al., 1995; Golchin et al., 1994). This finding led to the conclusion that degradation of organic residues reduces the O/N-alkyl C derived from preferential decomposition of carbohydrates (Baldock et al., 1992; Baldock and Skjemstad, 2000). Simultaneously, the increased contribution of alkyl C has been related to organic products synthesized within that fraction (Baldock et al., 1992) and selective preservation of these (Quideau et al., 2000). In clay-sized fractions, increasing contributions of alkyl C, and in some cases, of O/N-alkyl C, have been related to increased preservation of OM (Baldock et al., 1992; Schöning et al., 2005).

Here we investigate how soil texture affects microaggregation and how it controls the OM of microaggregates in the topsoil of an arable site in Scheyern (Germany). Size distributions enabled us to distinguish microaggregates as objects < 250 µm that can be dispersed into smaller building-particles. We show how aggregates in size fractions < 250 µm can be distinguished from particles and get a measure for the aggregate sizes by dynamic image analysis of wet-sieved and dispersed size fractions. This helps to determine precisely a wide size distribution of aggregates and particles between fine silt and sand size. A study of the entire microaggregate scale < 250 µm can directly resolve the role of fine particles in the formation of aggregates that can be several 100 µm larger than the building particles. This allows us to better understand how soil particles are structured in microaggregates and how different particle-size distributions affect aggregation. SSA measurements were included in our study to analyze whether SSA is related to OM stabilization by microaggregates. We employed solid-state ^{13}C NMR spectroscopy to determine the OM compositions of various size fractions to investigate the degree of OM decomposition. Our objectives were (i) to quantify the effect of soil texture on free and occluded size fractions, (ii) to differentiate the wet-sieved state from the dispersed ($Na_4P_2O_7$) state to identify preferential sizes of microaggregates, (iii) to compare the properties of OM in size fractions along a clay content gradient, and (iv) to test whether OM concentrations is interlinked with the SSA of the isolated size fractions.

2. Material and methods

2.1. Research site and sampling

The research site is located at the agricultural research station in Scheyern (Germany). Soil samples were taken from the same plot at five sites each with five independent samplings within 1–2 m of a radial sampling scheme (Wilding, 1985) as described by Krause et al. (2018). The locations of the five sites in the plot were determined systematically to represent increment ranges of clay content along the clay content gradient based on previous remote sensing studies (Sommer et al., 2003; Weller et al., 2007). The topsoil at depths of 5–20 cm was sampled with a large core cutter (3 dm^3). After sampling, the field-fresh samples were gently passed through an 8 mm sieve and stored at 4 °C. To isolate the bulk soil fraction, the dried soil sample was grinded with pestle and mortar until the whole sample passed through a 2 mm sieve. The isolation of free and occluded fractions in the microaggregate size range is described in section 2.2.

The entire plot has been subjected to similar management over decades of agricultural usage (Schröder et al., 2002). Further information about the potential C input can be gained from a remote sensing study from Sommer et al. (2003) on the same plot. The study analyzed the red and near-infrared canopy reflectance and related it to aboveground biomass during two winter wheat vegetation periods. Based on this data, we derived the wheat dry matter at the sampled sites within a square with 3 m edges. On average, the wheat dry matter was 1114 g m^{-2}. On the low-clay soils with a mean clay content of 19% and 22%, the dry matter was 89% (1032 g m^{-2}) compared to the high-clay soils with 32% and 34% clay (1159 g m^{-2}). From this background information on the dry matter differences, we can estimate that the low-clay soils received approximately 11% less C input from wheat harvest residues than the high-clay soils.

At the sampling site, the annual mean temperature is 7.4 °C, and the average annual precipitation is 803 mm at 464–482 m above sea level. A soil association of Cambisols developed on Miocene Upper Freshwater Molasse that is heterogeneously covered by Quaternary

Table 1
Textures of soil samples obtained from five sites (mean; range in brackets; $n = 5$) on the same agricultural plot after removal of organic matter with H_2O_2.

Sampling site	Clay content (< 2 µm)[a]	Silt content (2–53 µm)	Sand content (53–2000 µm)
1	18.7 (16.1–20.2)	19.5 (18.2–21.6)	61.7 (59.8–62.7)
2	22.1 (17.9–23.6)	21.6 (19.1–25.1)	56.3 (54.3–57.7)
3	24.2 (18.8–26.9)	25.8 (23–30.6)	50 (48.2–52.1)
4	32.3 (24.7–36)	38.7 (34.1–45.3)	29 (27.3–30)
5	34.3 (28.2–37.4)	44 (41.6–48.3)	21.6 (20.6–23.5)

[a] Data adapted from Krause et al. (2018).

loess. No lime application or calcium carbonate was found in the sampled soil material. The average soil pH of the entire toposequence was 5.2 ± 0.06, as determined in 0.01 M $CaCl_2$ solution at a mixing ratio of 1:2.5 soil:solution (m/v). The clay content of the top soils varied from 16 to 37% (Krause et al., 2018) (Table 1). Throughout the clay gradient, the clay mineral composition was generally dominated by Illite, accompanied by a low-to-moderate smectite and vermiculite contents (Karin Eusterhues and Pavel Ivanov, personal communication). The silt content increased linearly with clay content (Table 1). The differences between low-clay and high-clay soils are, thus, not limited to clay-sized particles but can also include silt-sized particles.

2.2. Isolation of microaggregate-sized soil fractions in water

The field-fresh soil samples were slowly submerged in water for 30 min and transferred to 250-µm and 53-µm sieves (Fig. 1). To isolate free size fractions, we moved the sieves 1 cm upward and downward at 30 rpm with the soil submerged in deionized water for 5 min. The isolated free size fractions on the 250-µm and 53-µm sieves were freeze-dried and stored at room temperature for analyses of OM and specific surface area. The soil remaining on the 250-µm sieve was sonicated at 60 J ml^{-1}, as described by Amelung and Zech (1999), to break the macroaggregates down to smaller aggregates that were occluded in the macroaggregates (Fig. 1). A Branson Sonifier 250 with a 13-mm tip was used for sonication (Branson Ultrasonics Corporation, Danbury, USA). Graf-Rosenfellner et al. (2018) showed that this sonication set up allows for a replicable determination of size fractions. The sonicated occluded size fractions were wet-sieved again with 250-µm and 53-µm sieves and the > 250 µm, 53–250 µm and < 53 µm fractions were recovered as described above. The sonicated occluded size fraction > 250 µm was dry-sieved with a 2 mm sieve to isolate the 'gravel' fraction > 2 mm which was weighed and subtracted from the sample weight.

2.3. Size distribution

The field-fresh soil samples were fractionated into free and occluded microaggregate-sized soil fractions, as described above, by using only a 250-µm sieve. The sizes of objects in the range of 11–250 µm were determined by means of dynamic image analysis where suspensions are pumped through a closed cycle with rear illumination from a pulsed laser light. We used a QICPIC machine (Sympatec GmbH, Clausthal-Zellerfeld, Germany), as described by Kayser et al. (2019). Directly after wet-sieving, the sample was washed into the basin of the SUCELL pump unit (Sympatec GmbH, Clausthal-Zellerfeld, Germany) from which a peristaltic pump drew the suspension at 9 ml s^{-1} through 4 mm tubes towards a cuvette with the imaging unit. The imaging unit measured the suspensions during 30 s, simultaneously with the start of the pump. According to preliminary trial results (Fig. S1), the pumping did not disrupt aggregates in the wet-sieved size fraction 53–250 µm. A previous study (Kayser et al., 2019) reported no measurable disruption of size fractions < 63 µm during several hours of pumping through the system. To prevent distortion of the size distribution because of air bubbles and root hair, we only included detected objects with a sphericity of 0.6–0.93. The particle sizes were quantified using the minimum Feret diameter, which describes the minimum distance of two tangents to the contours (Allen, 1981). To relate the size distribution to a mass distribution, it was determined as volumetric Q3 distribution. The Q3 distribution is a measure of the relative size fractions of solids in the suspension to the total sample approximating a mass distribution (based on the estimated volume and density of the solids, which was 2.65 g cm^{-3} in our case) according to the ISO norm for representation of results of particle size analysis (ISO 9276-1:, 1998). In addition to the size distribution of the samples submerged in deionized water, we determined the size distribution of the dispersed free and occluded fractions < 250 µm submerged in 1 M $Na_4P_2O_7$ followed by shaking and another sonication at 60 J ml^{-1}.

The size distribution in size range < 11 µm of the < 250-µm-sieved suspensions was determined by sedimentation and pipette analysis. At 20 °C room and water temperature, we pipetted 10 ml from the

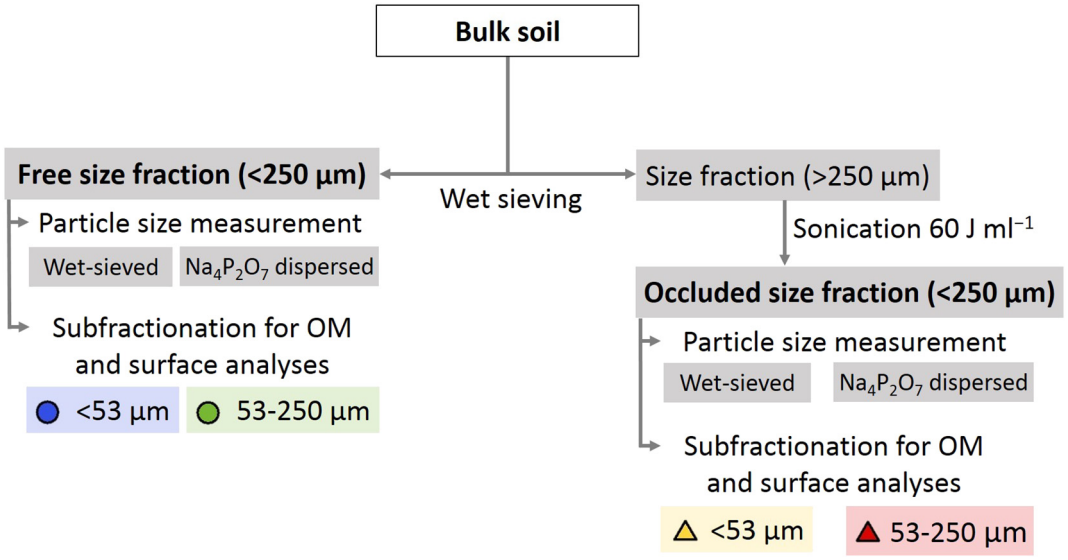

Fig. 1. Overview of isolation of free size fractions and those occluded in macroaggregates by using wet sieving and sonication. The size distributions were measured after wet-sieving and additional $Na_4P_2O_7$-dispersion to distinguish aggregates and non-aggregated particles in the size fractions. Further subfractions were isolated for OM and surface analyses.

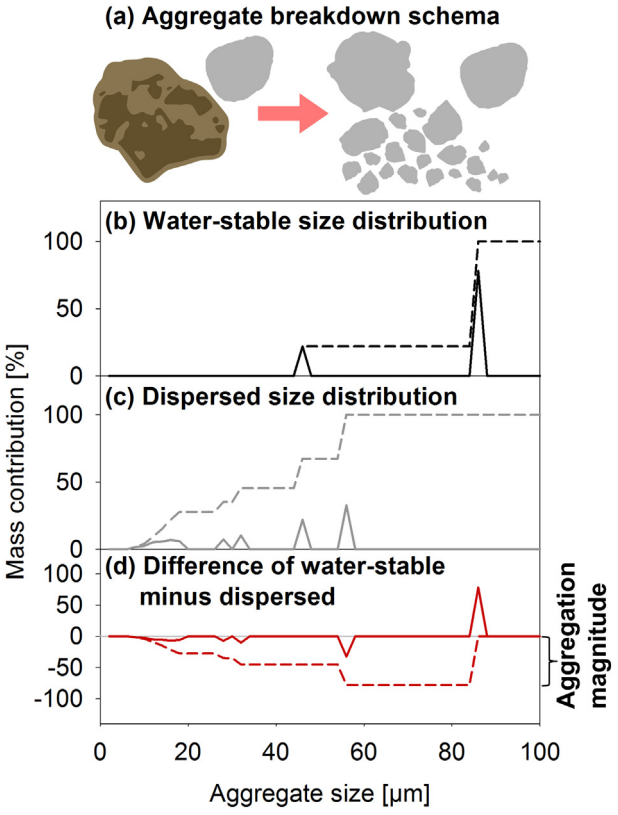

Fig. 2. (**a**) Schematic size distributions based on simplified theoretical scenario with one aggregate and one non-aggregated particle. Dynamic image analysis enabled us to resolve the size distribution of soil suspensions with a resolution of several µm. The size distributions are shown as frequency mass contribution (solid line) and cumulative mass contribution (dashed line). Determining size distributions in both (**b**) wet-sieved and (**c**) dispersed state (in this study $Na_4P_2O_7$ was used) enabled us to detect the size range in which there were aggregates that break down and the size range in which there were non-aggregated particles, as detected in both size distributions. (**d**) Difference of both distributions reveals the building units of aggregates (negative values) and true aggregates (positive values), whereas the non-aggregated particle is zero. The magnitude of the cumulative difference provides an estimate of the aggregation magnitude.

suspension in a 1 l cylinder at 10 cm depth after 15 min 20 s (< 11 µm fraction) and 46 min 43 s (< 6.3 µm fraction). At the depth of 5 cm, we pipetted after 3 h 52 min 48 s (< 2 µm fraction). The pipette fractions were dried at 105 °C for 24 h and weighed. The pipette fractions containing the $Na_4P_2O_7$-treated suspensions were corrected for $Na_4P_2O_7$ content. The size distributions of 11–250 µm obtained by dynamic image analysis and < 11 µm obtained by sedimentation and pipette analysis were merged weighed on the basis of their mass contribution of < 11 µm. The size distribution of < 250 µm was scaled based on their mass contribution to bulk soil. The difference of wet-sieved minus dispersed objects was used to correct for the content of primary particles in aggregates; a positive difference indicates true water-stable aggregates, whereas a negative difference indicates primary particles that are part of these aggregates (Fig. 2). This enables identifying the specific size ranges of unaggregated primary particles and aggregates, which can be dispersed into smaller building-particles (Fig. 2). In contrast to sieving methods, with dynamic image analysis particles and aggregates can be differentiated at a resolution of several µm. A similar difference of wet-sieved and sonicated minus dispersed objects was calculated for the occluded size fractions. The mean aggregate size $\bar{s}$ was calculated according to

$$\bar{s} = \frac{\sum_i^j m_i \cdot s_i}{\sum_i^j m_i}$$

where m_i is the mass contribution of size class i, and s_i is the mean size of size class i (applied to sizes 50–180 µm).

2.4. Organic matter analyses

As the soil material was carbonate-free, the OC and N concentrations of the size fractions were directly analyzed by means of dry combustion at 1000 °C by using a Vario EL 315 CN analyzer (Elementar, Langenselbold, Germany). To determine the chemical composition of the OM in the size fractions, we used solid-state ^{13}C NMR spectroscopy. We employed a Bruker DSX 200 NMR spectrometer (Bruker, Billerica, USA) at a resonance frequency of 50.3 MHz with the cross-polarization magic angle spinning technique (CP-MAS). The samples were spun at 6.8 kHz and analyzed with a pulse delay of 400 ms. We quantified the chemical shift regions by integrating at 0–45 ppm (alkyl C), 45–110 ppm (O/N-alkyl C), 110–160 ppm (aryl C), and 160 to 220 ppm (carboxyl C), including spinning side bands (Knicker et al., 2005).

2.5. Specific surface analysis with N_2-BET

To determine the SSA of the size fractions, we employed multi-point BET (Brunauer et al., 1938) by using an Autosorb-1 analyzer (Quantachrome, Syosset, USA) with N_2 gas as adsorbate at 77 K. The samples were prepared by outgassing them under vacuum by using helium at 40 °C for 12 h.

To remove OM from the size fractions, we mixed them four times for 24 h at 1:50 with 1 M NaOCl (pH 8). We washed the soil with deionized water until < 50 µS cm^{-1}, freeze-dried the material, and analyzed its SSA. The difference of the SSA of the unoxidized sample minus the SSA after oxidation provided a measure of the SSA loaded with OM (SSA_{OM}; $m^2\,g^{-1}$). We assumed the SSA of the surfaces covered with OM was negligible, as indicated in the literature (Heister, 2014; Kaiser and Guggenberger, 2007).

2.6. Statistics

We used a linear model in R (Rstudio 1.1.447) to determine the relationship between clay content and the mass contribution of size fractions or the mean aggregate size. According to the radial sampling at five sites along the clay content gradient, each with five independent samples at a closer proximity, we accounted for the disparate spatial scales with a nested site factor (Webster and Lark, 2013). We used SigmaPlot 11 to test for normality (Shapiro–Wilk test) and equal variances. We analyzed the alkyl:O/N-alkyl ratio with a two-way analysis of variances in R (Rstudio 1.1.447) including the 3 clay content sites and 5 size fractions. As the interaction factor and the clay content site factor were not significant ($p > 0.05$), we compared the means of the significant fraction factor by conducting a Tukey test.

3. Results

3.1. Aggregate and particle-size distributions

The size distribution within the free fraction < 250 µm differed depending on the clay content: There were fewer > 100 µm objects in the high-clay soils than in the low ones (Fig. 3a). After chemical dispersion, the mass contribution of < 6.3 µm objects increased (Fig. 3c), whereas the increased proportion of > 100 µm objects in the low-clay soils remained enabling to distinguish them as primary particles. By summarizing the size distribution after dispersion in three textural size classes, we observed that in the free fraction of the low-clay soils there were more fine sand particles > 100 µm and 5% less clay-sized particles

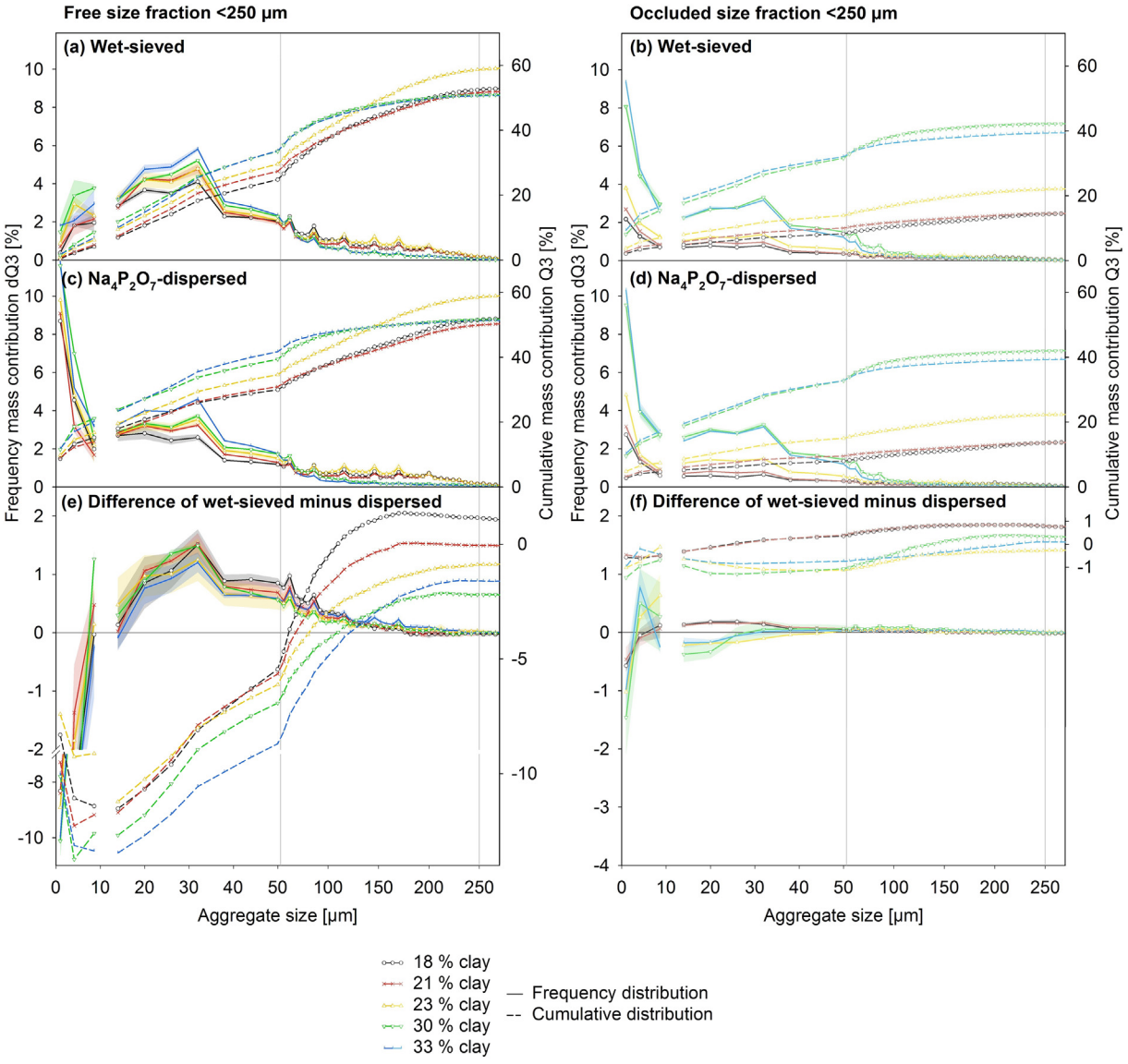

Fig. 3. Size distributions obtained from combined pipette and dynamic image analysis of (**a**, **c**, **e**) free and (**b**, **d**, **f**) occluded size fractions of < 250 µm scaled to their mass contributions to the bulk soil (Fig. 5a). Five sites with different clay contents are shown as frequency distributions (mean ± standard error; n = 3) and cumulative distributions (mean; n = 3). The size fractions were analyzed in (**a**, **b**) water and (**c**, **d**) after dispersion in $Na_4P_2O_7$, by means of dynamic image analysis. (**e**, **f**) Difference of wet-sieved minus dispersed distributions shows the true aggregates as positive and building particles as negative.

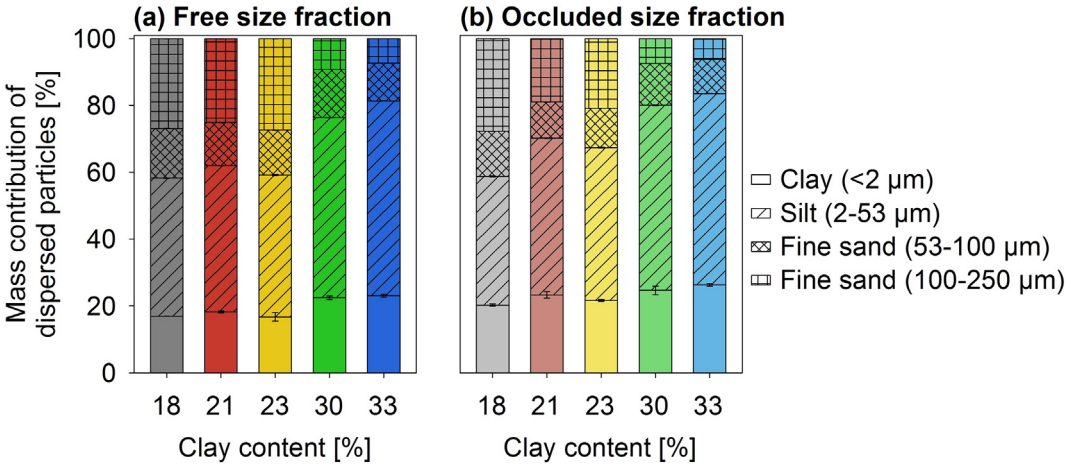

Fig. 4. Mass contribution of particle-size classes in (**a**) free fraction < 250 µm, as deduced from Fig. 3c, and (**b**) occluded fraction < 250 µm, as deduced from Fig. 3d.

Table 2
Mean size of difference of wet-sieved minus dispersed objects in the size range 50–180 µm (mean ± standard error; $n = 3$).

Mean clay content (%)	Mean size (µm)	
	Free fraction	Occluded fraction
18	84.6 ± 2.4	91.5 ± 1.8
21	88.6 ± 1.4	85.9 ± 4.8
23	90.1 ± 1.9	101.7 ± 0.7
30	92.1 ± 1	104.7 ± 5.8
33	95.8 ± 1.4	107.4 ± 1.4

compared to the high-clay soils (decrease from 22.8 to 17.6% clay) (Fig. 4a). When excluding the sand-sized particles > 100 µm, the texture of the free fraction was found to be similar for all clay contents (Fig. S2). The difference of wet-sieved minus dispersed objects indicated that most microaggregates measured approximately 30 µm in diameter (Fig. 3e). The mass contribution of the > 30 µm aggregates decreased with their size (Fig. 3e). Increasing clay content showed a positive relationship to the mean size in the 50–180 µm size range ($R^2 = 0.71$; $p = 0.028$; $n = 15$; Fig. 3e; Table 2).

After weak sonication of the size fraction > 250 µm, approximately 13–17% of the bulk soil was < 6.3 µm in the occluded fraction (Fig. 3b). The occluded fraction contained 23.3% clay-sized particles, which is 4% more than in the free fraction (Fig. 4). The texture of free and occluded fractions resembled each other in comparable patterns: The low-clay soils contained a higher proportion of fine sand particles > 100 µm and 4% lower clay content compared to the high-clay soils (decrease from 25.5 to 21.8% clay) (Fig. 4b). The difference of wet-sieved minus dispersed objects of the occluded fractions was 10 times lower than that of the free fraction (Fig. 3f). The mean size at 50–180 µm of the difference of occluded wet-sieved minus dispersed objects showed a positive relationship to clay content ($R^2 = 0.69$; $p = 0.033$; n = 15; Fig. 3f; Table 2). The soils showed contrasting patterns in the finer size range. In the two low-clay soils (18 and 21% clay), the diameter of most of the occluded microaggregates was approximately 23 µm (Fig. 3f). Occluded aggregates of the high-clay soils dispersed into building units measuring approximately 20 µm, whereas the aggregates of the low-clay soils dispersed into building units measuring < 6.3 µm (Fig. 3f).

The wet sieving fractionation of the size fractions showed a positive relationship of increasing clay content to the mass contribution of the free size fraction < 53 µm to the bulk soil ($R^2 = 0.90$; $p < 0.001$; $n = 23$). The relationship of clay content to the contribution of the fraction 53–250 µm was negative ($R^2 = 0.61$; $p = 0.005$; n = 23; Fig. 5a). In the occluded fraction, clay content showed a positive relationship to both size fractions (< 53 µm: $R^2 = 0.87$; $p < 0.001$; $n = 24$; 53–250 µm: $R^2 = 0.67$; $p < 0.001$; n = 24; Fig. 5a). Taken together, the mass contribution of the occluded fractions increased from approximately 15 to 40% of the bulk soil (Fig. 5a).

3.2. Organic matter in size fractions

In the bulk soil, the average OC concentration was higher in the high-clay soils (14 mg OC g^{-1} at 33% clay) than in the low-clay soils (12 mg OC g^{-1} at 20% clay, Fig. 5b). The OC and N concentrations of the free and occluded < 53 µm fractions of the low-clay soils were higher than those of the high-clay soils (Fig. 5b, c). The larger 53–250 µm fraction showed similar OC and N concentrations for all clay contents in the free and the occluded fractions (Fig. 5b, c). The C:N ratios of the large 53–250 µm fractions were generally higher than that of the small < 53 µm fractions (around 8 for the free and the occluded small fractions), and it did not show any trend with the clay content. The occluded size fractions had a higher C:N ratio of approximately 18 compared to the free size fractions, which had a C:N ratio of approximately 12 (Fig. 5d). The relative OC contributions of the free aggregate size fractions to the bulk soil OC decreased whereas that of the occluded fractions increased with increasing clay content (Fig. 5e).

Our analysis of the OM composition revealed that the < 53 µm fractions were characterized by more alkyl and less O/N-alkyl C, resulting in a higher alkyl:O/N-alkyl C ratio than those of the 53–250 µm fractions and the bulk soil (Table 3). The free < 53 µm fraction had a higher alkyl:O/N-alkyl ratio and a higher proportion of carboxyl C than those of the occluded fraction (Table 3). The 53–250 µm fractions did not differ from each other and from the bulk soil. There was no trend with increasing clay content (Table S1).

3.3. Specific surface area and surface loading of organic carbon

The SSA of the bulk soil increased from 5.2 to 9.3 $m^2 g^{-1}$ with increasing clay content (Fig. 6a). By contrast, the SSA of the size fractions remained constant across all analyzed clay contents (Fig. 6a). The SSA of the < 53 µm fractions was higher than that of the 53–250 µm fractions (Fig. 6a). When removing the OM via NaOCl oxidation, the SSA difference of the oxidized minus the unoxidized sample (SSA_{OM}) indicated the SSA loaded with OM. SSA_{OM} decreased from 14 to 8 $m^2 g^{-1}$ for the free size fraction and from 20 to 14 $m^2 g^{-1}$ for the occluded size fraction measuring < 53 µm (Fig. 6b). The OC concentrations of the fractions showed a positive relationship to SSA_{OM} (free $_{< 53\ \mu m}$: $R^2 = 0.72$; $p = 0.039$; $n = 14$; occluded $_{< 53\ \mu m}$: $R^2 = 0.95$; $p = 0.008$; $n = 9$).

4. Discussion

4.1. Soil texture control over aggregation

The dynamic image analysis of size fractions pumped through a closed suspension cycle facilitated size-specific observations of water-stable aggregate structures and their building particles. Resolving the confounding effect of soil aggregation on the distribution of particles and OM provides novel insights that extend our knowledge, which was mostly obtained by mass comparisons of size fractions. A synthesis of our results is presented in a schematic summary in Fig. 7.

It is important to differentiate particles and aggregates when comparing the aggregation between soils with different textures. The effect of increasing mass contributions of fine particles depends on whether these particles participate in aggregation and which aggregate sizes they build. The differentiation of wet-sieved size distributions from dispersed distributions enabled us to determine that mostly free microaggregates of approximately 30 µm diameter were formed at a similar proportion in the soils independently from the clay content gradient (Fig. 3e). The stimulative effect of soil clay content on mass contributions of water-stable aggregated soil structures was, therefore, decoupled from a higher mass contribution of true aggregates and rather related to larger aggregate sizes. The differentiation of aggregate size distributions and particle size distributions revealed a 15% higher contribution of sand-sized particles > 100 µm to the size fractions of low-clay soils (18–21% clay content), which did not form part of water-stable aggregates (Figs. 3c, d; 4). Instead, the size fractions contained similar size distributions of particles < 100 µm from all soils, irrespective of the clay content (Fig. S2). This indicates the integration of a prevailing fine particle size distribution in the free microaggregates independent of the bulk soil clay content. A similar prevailing particle size distribution independent of clay contents corroborates a constant ratio of clay-to-silt-sized particles for the size fraction < 53 µm (Balabane and Plante, 2004). By contrast, we observed that different silt and clay particle size distributions mostly affected the size distribution within larger aggregates > 53 µm (Table 2). This is reflected in the unimodal right-skewed distribution pattern of the differentiated wet-sieved and dispersed size distributions, whereas the long right tail of the distribution shows varying contributions of aggregates measuring

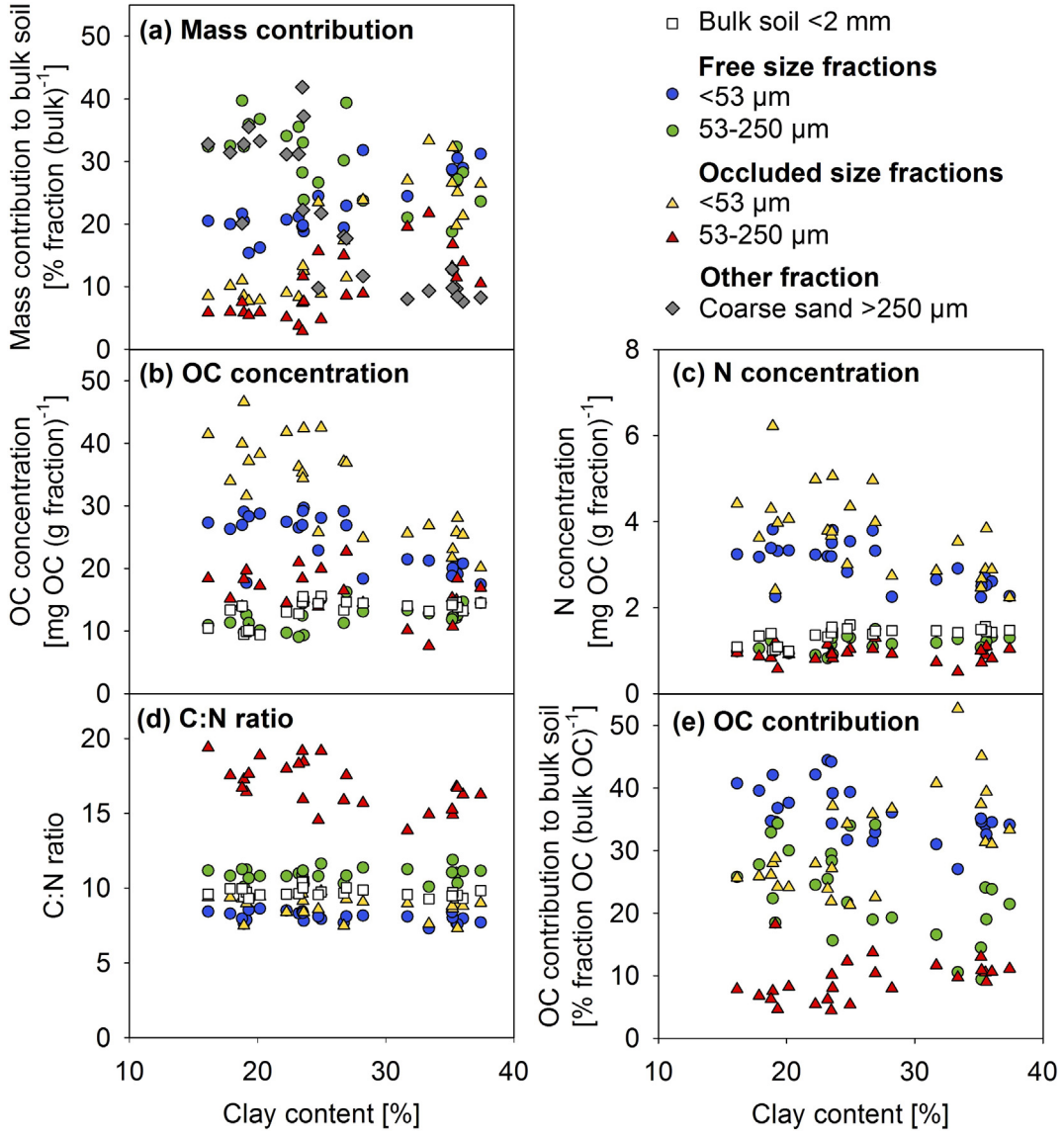

Fig. 5. (**a**) Mass contributions of size fractions to bulk soil, (**b**) OC concentration, (**c**) N concentration, (**d**) C:N ratio, and (**e**) their relative OC contributions.

Table 3
Integrals of functional C groups in solid-state ^{13}C CP-MAS NMR spectra (summarized for three different clay contents; mean ± standard error; n = 3). The soils were fractionated into free and occluded aggregate size fractions. Data of individual clay contents are given in Table S1 and Fig. S3. Values with the same letter within one column are not significantly different (p = 0.05).

Fraction	Size	Alkyl C (%)	O/N-alkyl C (%)	Aryl C (%)	Carboxyl C (%)	Alkyl:O/N-alkyl ratio
						ANOVA p < 0.001
Bulk	< 2 mm	14.1 ± 0.3	47.3 ± 0.4	25.8 ± 0.5	12.4 ± 0.7	0.30 ± 0.02 a,b
Free	< 53 µm	21 ± 0.6	42.7 ± 0.7	21.7 ± 1.2	13.7 ± 1.2	0.5 ± 0.01 c
Free	53–250 µm	14.3 ± 1.2	46 ± 2.1	27 ± 0.6	12 ± 1	0.32 ± 0.03 a,b
Occluded	< 53 µm	18.3 ± 0.9	48.3 ± 0.7	22.7 ± 0.9	10.3 ± 0.3	0.38 ± 0.02 b
Occluded	53–250 µm	13.3 ± 1.3	49.7 ± 1.8	26.7 ± 0.7	10 ± 1.5	0.27 ± 0.03 a

50–180 µm (Fig. 3c).

In the macroaggregates > 250 µm, sand-sized particles were occluded to a similar extent as in case of the free microaggregates, but the macroaggregates contained 4% more clay (Fig. 4). This indicates that when embedded in larger structures, the aggregate building units can have a broad size range, including sand-sized particles. Obviously, the higher proportion of clay-sized particles was crucial for building larger aggregates. This means that a minor part of the clay-sized building units had a stabilizing effect on larger aggregate structures. The more clay-rich particle-size distribution of the wet-sieved size fractions > 250 µm compared to that of the microaggregates explains the higher mass contributions of larger soil structures in the high-clay soils (Fig. 5a).

Higher mass contributions of clay- and silt-sized particles did not lead to formation of a greater number of clay- and silt-sized aggregates, but instead led to the formation of aggregates with higher mean sizes in the 50–180 µm range, as detected by the differentiation of wet-sieved

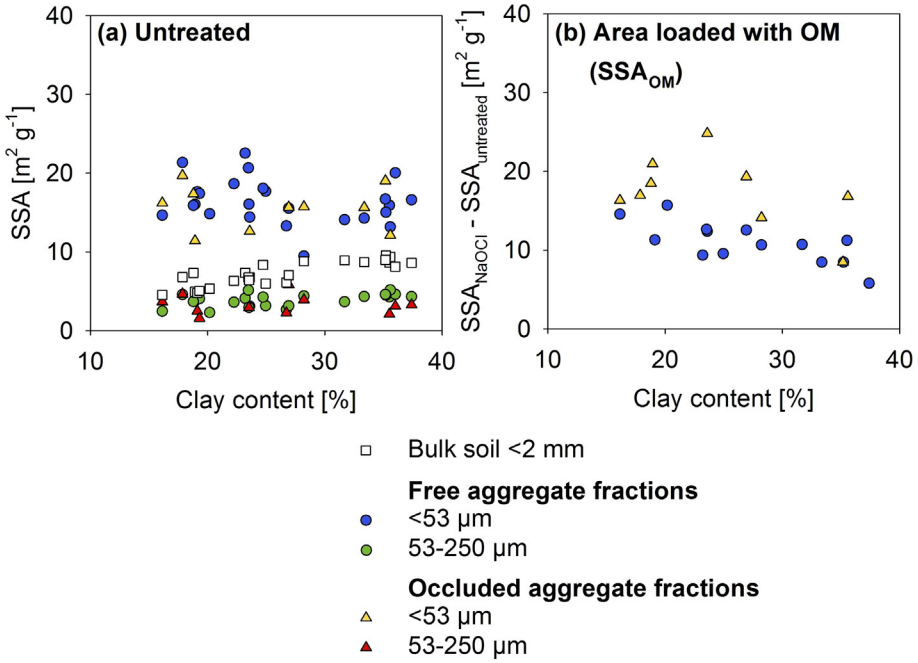

Fig. 6. Specific surface area (SSA; measured with N_2-BET) of (**a**) untreated size fractions, reflecting the remaining surface. (**b**) Area loaded with OM by calculating the difference between SSAs of NaOCl-treated sample and untreated sample (SSA_{OM}).

and dispersed size distributions (Table 2). The presence of a higher contribution of sand-sized particles > 100 µm might have hampered the buildup of larger aggregate structures, as observed in the low-clay soils.

Through weak sonication of the wet-sieved macroaggregates, we isolated a size fraction that contained microaggregates occluded previously in the larger soil structures. In a comparison of the cumulative difference between the wet-sieved size distribution and the dispersed size distribution, we found that the aggregation magnitude of the occluded microaggregates was 10 times lower than that of the free microaggregates (Fig. 3f). A direct breakdown of the macroaggregates to dispersed particles during sonication indicates that the potentially occluded microaggregates did not resist the sonication. However, for both the free and the occluded microaggregates, we found positive correlations of larger diameters of true aggregates with increasing clay content (Table 2).

4.2. Organic matter distribution as governed by aggregation

The mean OC concentration in the bulk soil of the high-clay soils (14 mg OC g^{-1} at 33% clay) was slightly higher than the bulk OC concentration of the low-clay soils (12 mg OC g^{-1} at 20% clay; Fig. 5b). As estimated in section 2.1 based on a remote sensing study of the same plot (Sommer et al., 2003), the C input from crop residues was probably approximately 11% higher in the high-clay soils than in the low-clay soils. Many previous studies have related high-clay soils with higher OC concentrations owing to more mineral-associated OC (Laganière et al., 2010; Stewart et al., 2007). In contrast to most of these studies, here we could compare soils with different clay contents from the same plot and similar management. This excludes potentially confounding factors such as different climate, management, or pedogenesis. However, the relationship between the soil clay content and OM concentrations as well as inputs could not be completely disaggregated on the sampled plot. In this study, the slightly increasing bulk soil OC concentrations along the clay content gradient might have enhanced the differences

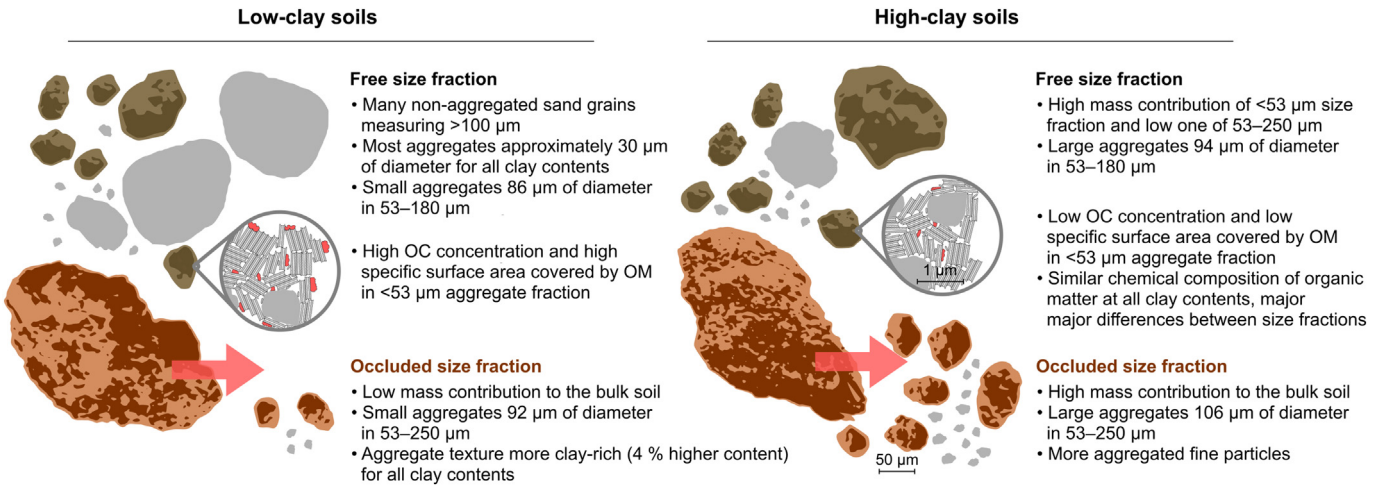

Fig. 7. Schematic summary based on Table S2. All comparisons are between clay contents, if not noted otherwise.

between the OC concentrations of the isolated size fractions to a small extent: the OC concentrations in both the free and the occluded size fractions < 53 µm decreased with decreasing clay content, whereas they remained constant in the 53–250 µm size fractions (Fig. 5b).

The OC concentrations of the size fractions diverged from their mass contributions: the mass contributions of both the free and the occluded size fractions < 53 µm decreased with decreasing clay content, whereas their OC concentrations increased (Fig. 5b). The increased mass contribution of the size fraction < 53 µm owing to higher contributions of clay and silt particles probably led to the lower OC concentration through dilution.

Our finding that mineral particle-size distribution controls aggregation instead of the OC concentration is in contrast to the postulated stabilization of soil structure with increasing OM concentration (Dexter et al., 2008; Jensen et al., 2019; Schjønning et al., 2012). The studies referenced above used clay dispersibility as an indicator of soil structure stabilization. We observed that higher contents of particles > 100 µm led to the formation of smaller aggregates at the sand-size scale (Fig. 4). The influence of such large primary particles necessitates extending assessment over the entire size scale of microaggregation < 250 µm. Our data shows how the presence of only a few more clay-sized particles enhanced soil aggregation. A higher proportion of clay-sized particles enabled the buildup of a greater number of clay-rich macroaggregates in high-clay soils.

The OC concentrations in the < 53 µm size fractions were higher than those in the 53–250 µm size fraction (Fig. 5b). This coincides with the higher SSA of the smaller size fraction (Fig. 6a), which is governed by a finer size distribution (Petersen et al., 1996). A higher SSA has been frequently related to enhanced OM stabilization through surface adsorption (Baldock and Skjemstad, 2000; Jones and Edwards, 1998). The SSA within the individual size fractions remained constant across all analyzed clay contents (Fig. 6a) reflecting the similar size distributions of particles < 100 µm throughout the clay content gradient (Fig. 4). The constant SSA of the untreated fractions was decoupled from changes in the OM concentrations. The additional mineral surface area after OM removal served as a more correlative indicator (Fig. 6b). Higher SSA_{OM} and OC concentrations in the < 53 µm size fraction of the low-clay soils could be related to higher aggregate proportions in the size fractions < 53 µm and a potential dilution of aggregates with non-aggregated fine particles in the high-clay soils. That the increased OC concentrations in the < 53 µm size fraction coincided with the buildup of smaller aggregates in the low-clay soils shows that smaller structural units did not necessarily limit OM stabilization.

4.3. Microaggregation and chemical composition of organic matter

In contrast to the changes in the OC concentration with clay content, the chemical composition of OM in the size fractions did not differ significantly with clay content, according to solid-state ^{13}C NMR spectroscopy (Table S1, Fig. S3). The N concentration, too, followed a similar pattern as the OC, resulting in constant C:N ratios over the entire range of clay content.

In a comparison of the size fractions, we found a higher contribution of alkyl and a lower contribution of O/N-alkyl C, resulting in higher alkyl:O/N-alkyl ratios in the < 53 µm fractions than that in the 53–250 µm fractions (Table 3). This indicates a higher level of degradation of OM in the smaller fractions, as reflected by the low C:N ratio of approximately 8 of the < 53 µm fractions (Fig. 5d). The decreasing C:N ratio of the small size fraction within < 250 µm aggregates was corroborated by the results of an earlier study on a Luvisol under agricultural land use (Fernández-Ugalde et al., 2013). The present study confirmed this size-dependent C:N relationship for microaggregates occluded in macroaggregates as well, whereas this relationship was weaker in the case of intact macroaggregates in Fernández-Ugalde et al. (2013). Previous studies have related the higher contribution of alkyl C to increased microbial processing of OM in the fine fractions (Baldock et al., 1992; Schöning et al., 2005; Yu et al., 2015). Higher contributions of carboxyl C in the free size fractions indicate that these functional groups are related to aggregate stabilization through deprotonation (Kleber et al., 2007). Carboxyl C seems to be more important in free microaggregates compared to occluded ones at the neutral-to-slightly acid pH ($CaCl_2$) of 5.2. The significantly higher C:N ratios of the occluded large size fractions measuring 53–250 µm point to the higher contribution of non-proteinaceous OM in these fractions. This is most probably because of the incorporation of plant-derived particulate OM with a generally high C:N ratio. This observation is consistent with the lower degree of OM degradation as indicated by the alkyl:O/N alkyl ratio of 0.27 (Table 3). A previous study on the same experimental site showed that the OC contribution of free particulate OM was approximately 2.5% of the bulk soil OC whereas the occluded particulate OM contributed 4.5 to 9% of the bulk soil OC (Kölbl and Kögel-Knabner, 2004). This showed that the majority of the OC contributions from particulate OM are occluded in aggregates, which hampers its removal from aggregates in the size fraction. The distribution of particulate OM within the isolated size fractions < 250 µm could influence the OC concentrations. Most of the OC contributions from particulate OM seem to be contained in the occluded size fractions based on their lower alkyl:O/N alkyl ratios compared to the free size fractions (Table 3).

The OC concentrations and the C:N ratios of the occluded fractions were higher than those of the free fractions, whereas their alkyl:O/N-alkyl ratios were lower (Table 3; Fig. 5b, d). These differences indicate increasing preservation of the occluded OM, which is decoupled from the mineral surface area that was found to depend mostly on the mineral particle-size distribution of the aggregates (Fig. 5b, c). Decreasing C:N ratios could be related to a higher amount of mineral-fixed ammonium as well, which has been shown to be correlated positively the clay content (Jensen et al., 1989). Although the size fractions contained higher proportions of clay- and silt-sized particles with increasing clay content, the C:N ratios did not differ. This indicates that the observed C:N ratios were mostly related to the decomposition of OM instead of the mineral-fixed ammonium.

A compelling number of studies have related finer soil texture to increased OM stabilization in soils (Stewart et al., 2008; Wiesmeier et al., 2019). In our study, the dominating differences between size fractions instead of those between soil clay contents show that the OM stabilization was mostly mediated by the protection of OM in aggregates. These results are consistent with those of Fernández-Ugalde et al. (2016), who did not observe a clear relationship between contrasting mineralogy and the concentration and incorporation of OC among size fractions. The accumulation of swelling clay mineral phases in aggregates, as postulated by Fernández-Ugalde et al. (2013), might be overwritten when the particles combine into larger aggregate structures, as indicated by the prevailing texture pattern < 100 µm. The association of OM with the fine fractions of soils goes beyond the sorptive association of OM on mineral surfaces, and it cannot be understood without considering the effects of mineral particle aggregation. In our study, the strong differences between the OC concentrations of the size fractions show that the mass proportion of the size fractions are important for the OM stabilization. The influence of aggregation on the OM distribution within size fractions decoupled OM stabilization from the direct influence of soil texture.

5. Conclusions

By differentiating aggregate size distributions from their dispersed particle sizes, we quantified how soil texture governs the fragmentation of soil structure into different aggregated structures. High clay contents stimulated larger aggregate sizes, which could be hampered in the presence of higher proportions of non-aggregated sand-sized particles > 100 µm. A similar size distributions of particles < 100 µm in size fractions from the soils with widely differing clay contents indicated a prevailing pattern of the needed fine particles for aggregation.

A higher proportion of clay-sized particles was crucial for the buildup of larger aggregates. The smaller aggregates in the soils with fewer clay-sized particles did not prevent but instead did explain their higher OM concentrations. The diverging trends of the mass contributions of aggregate size fractions and their OM concentrations indicated that aggregation is governed by the mineral particle-size distribution instead of OM content. The chemical composition of OM was affected mostly by the size fraction, whereas the clay content had no influence. Soil texture was found to exert substantial control over the buildup of aggregates of specific sizes and the differing mass contributions of size fractions. The arrangement of mineral particles and OM in the soil structures is mostly controlled by a combination of different microaggregate sizes, aggregate mass proportions, and their underlying building particle-size distributions.

Acknowledgments

We thank Franziska Steiner, Sandra Bierbach, and Gilles Kayser for their technical assistance and Werner Häusler for his helpful advice. The insightful comments and helpful suggestions of the editor and two anonymous reviewers are gratefully acknowledged. We acknowledge the financial support by the Deutsche Forschungsgemeinschaft within the framework of the research unit "MAD Soil - Microaggregates: Formation and turnover of the structural building blocks of soils" (DFG RU 2179) through project KO 1035/48-1. The QICPIC machine was funded by the Deutsche Forschungsgemeinschaft (LA 1398/10-1).

Appendix A. Supplementary data

Supplementary data to this article can be found online at https://doi.org/10.1016/j.geoderma.2019.113901.

References

Allen, T., 1981. Particle Size Measurement, Powder Sampling and Particle Size Measurement Methods. Chapmann & Hall, London.
Amelung, W., Zech, W., 1999. Minimisation of organic matter disruption during particle-size fractionation of grassland epipedons. Geoderma 92 (1–2), 73–85.
Angers, D.A., Recous, S., Aita, C., 1997. Fate of carbon and nitrogen in water-stable aggregates during decomposition of $^{13}C^{15}N$-labelled wheat straw in situ. Eur. J. Soil Sci. 48, 295–300.
Bailey, V.L., Bond-Lamberty, B., DeAngelis, K., Grandy, A.S., Hawkes, C.V., Heckman, K., Lajtha, K., Phillips, R.P., Sulman, B.N., Todd-Brown, K.E.O., Wallenstein, M.D., 2018. Soil carbon cycling proxies: understanding their critical role in predicting climate change feedbacks. Glob. Chang. Biol. 24 (3), 895–905.
Balabane, M., Plante, A.F., 2004. Aggregation and carbon storage in silty soil using physical fractionation techniques. Eur. J. Soil Sci. 55 (2), 415–427.
Baldock, J.A., Skjemstad, J.O., 2000. Role of the soil matrix and minerals in protecting natural organic materials against biological attack. Org. Geochem. 31 (7–8), 697–710.
Baldock, J.A., Oades, J.M., Waters, A.G., Peng, X., Vassallo, A.M., Wilson, M.A., 1992. Aspects of the chemical structure of soil organic materials as revealed by solid-state ^{13}C NMR spectroscopy. Biogeochemistry 16 (1), 1–42.
Barré, P., Durand, H., Chenu, C., Meunier, P., Montagne, D., Castel, G., Billiou, D., Soucémarianadin, L., Cécillon, L., 2017. Geological control of soil organic carbon and nitrogen stocks at the landscape scale. Geoderma 285, 50–56.
Brunauer, S., Emmett, P.H., Teller, E., 1938. Adsorption of gases in multimolecular layers. J. Am. Chem. Soc. 60 (2), 309–319.
Carter, M.R., Angers, D.A., Gregorich, E.G., Bolinder, M.A., 2003. Characterizing organic matter retention for surface soils in eastern Canada using density and particle size fractions. Can. J. Soil Sci. 83 (1), 11–23.
Christensen, B.T., 1992. Physical fractionation of soil and organic matter in primary particle size and density separates. Adv. Soil Sci. 20, 1–90.
Dexter, A.R., Richard, G., Arrouays, D., Czyż, E.A., Jolivet, C., Duval, O., 2008. Complexed organic matter controls soil physical properties. Geoderma 144 (3), 620–627.
Elliott, E.T., Palm, C.A., Reuss, D.E., Monz, C.A., 1991. Organic matter contained in soil aggregates from a tropical chronosequence: correction for sand and light fraction. Agric. Ecosyst. Environ. 34 (1), 443–451.
Fernández-Ugalde, O., Barré, P., Hubert, F., Virto, I., Girardin, C., Ferrage, E., Caner, L., Chenu, C., 2013. Clay mineralogy differs qualitatively in aggregate-size classes: clay-mineral-based evidence for aggregate hierarchy in temperate soils. Eur. J. Soil Sci. 64 (4), 410–422.
Fernández-Ugalde, O., Barré, P., Virto, I., Hubert, F., Billiou, D., Chenu, C., 2016. Does phyllosilicate mineralogy explain organic matter stabilization in different particle-size fractions in a 19-year C3/C4 chronosequence in a temperate Cambisol? Geoderma 264, 171–178.
Ghezzehei, T.A., Or, D., 2000. Dynamics of soil aggregate coalescence governed by capillary and rheological processes. Water Resour. Res. 36 (2), 367–379.
Golchin, A., Oades, J.M., Skjemstad, J.O., Clarke, P., 1994. Soil structure and carbon cycling. Soil Res. 32 (5), 1043–1068.
Golchin, A., Clarke, P., Oades, J., Skjemstad, J., 1995. The effects of cultivation on the composition of organic-matter and structural stability of soils. Soil Res. 33 (6), 975–993.
Graf-Rosenfellner, M., Cierjacks, A., Kleinschmit, B., Lang, F., 2016. Soil formation and its implications for stabilization of soil organic matter in the riparian zone. Catena 139, 9–18.
Graf-Rosenfellner, M., Kayser, G., Guggenberger, G., Kaiser, K., Büks, F., Kaiser, M., Mueller, C.W., Schrumpf, M., Rennert, T., Welp, G., Lang, F., 2018. Replicability of aggregate disruption by sonication—an inter-laboratory test using three different soils from Germany. J. Plant Nutr. Soil Sci. 181 (6), 894–904.
Heister, K., 2014. The measurement of the specific surface area of soils by gas and polar liquid adsorption methods—limitations and potentials. Geoderma 216, 75–87.
ISO 9276-1, 1998. Representation of Results of Particle Size Analysis—Part 1: Graphical Representation.
Jastrow, J.D., Boutton, T.W., Miller, R.M., 1996. Carbon dynamics of aggregate-associated organic matter estimated by carbon-13 natural abundance. Soil Sci. Soc. Am. J. 60 (3), 801–807.
Jensen, E.S., Christensen, B.T., Sørensen, L.H., 1989. Mineral-fixed ammonium in clay- and silt-size fractions of soils incubated with 15N-ammonium sulphate for five years. Biol. Fertil. Soils 8 (4), 298–302.
Jensen, J.L., Schjønning, P., Watts, C.W., Christensen, B.T., Peltre, C., Munkholm, L.J., 2019. Relating soil C and organic matter fractions to soil structural stability. Geoderma 337, 834–843.
Jones, D.L., Edwards, A.C., 1998. Influence of sorption on the biological utilization of two simple carbon substrates. Soil Biol. Biochem. 30 (14), 1895–1902.
Kaiser, K., Guggenberger, G., 2007. Sorptive stabilization of organic matter by microporous goethite: sorption into small pores vs. surface complexation. Eur. J. Soil Sci. 58 (1), 45–59.
Kayser, G., Graf-Rosenfellner, M., Schack-Kirchner, H., Lang, F., 2019. Dynamic imaging provides novel insight into the shape and stability of soil aggregates. Eur. J. Soil Sci. 70 (3), 454–465.
Kemper, W.D., Chepil, W.S., 1965. Size distribution of aggregates. In: Black, C.A. (Ed.), Methods of Soil Analysis: Part 1. Agronomy, pp. 499–510.
Kleber, M., Sollins, P., Sutton, R., 2007. A conceptual model of organo-mineral interactions in soils: self-assembly of organic molecular fragments into zonal structures on mineral surfaces. Biogeochemistry 85 (1), 9–24.
Knicker, H., González-Vila, F.J., Polvillo, O., González, J.A., Almendros, G., 2005. Fire-induced transformation of C- and N-forms in different organic soil fractions from a Dystric Cambisol under a Mediterranean pine forest (Pinus pinaster). Soil Biol. Biochem. 37 (4), 701–718.
Kölbl, A., Kögel-Knabner, I., 2004. Content and composition of free and occluded particulate organic matter in a differently textured arable Cambisol as revealed by solid-state ^{13}C NMR spectroscopy. J. Plant Nutr. Soil Sci. 167 (1), 45–53.
Krause, L., Rodionov, A., Schweizer, S.A., Siebers, N., Lehndorff, E., Klumpp, E., Amelung, W., 2018. Microaggregate stability and storage of organic carbon is affected by clay content in arable Luvisols. Soil Tillage Res. 182, 123–129.
Laganière, J., Angers, D.A., Paré, D., 2010. Carbon accumulation in agricultural soils after afforestation: a meta-analysis. Glob. Chang. Biol. 16 (1), 439–453.
Mayer, L.M., Xing, B., 2001. Organic matter–surface area relationships in acid soils. Soil Sci. Soc. Am. J. 65 (1), 250–258.
Oades, J.M., 1984. Soil organic matter and structural stability: mechanisms and implications for management. Plant Soil 76 (1–3), 319–337.
Oades, J.M., 1988. The retention of organic matter in soils. Biogeochemistry 5 (1), 35–70.
Oades, J.M., 1993. The role of biology in the formation, stabilization and degradation of soil structure. Geoderma 56 (1–4), 377–400.
Paradiś, A., Brueck, C., Meisenheimer, D., Wanzek, T., Dragila, M.I., 2017. Sandy soil microaggregates: rethinking our understanding of hydraulic function. Vadose Zone J. 16 (9).
Petersen, L.W., Moldrup, P., Jacobsen, O.H., Rolston, D.E., 1996. Relations between specific surface area and soil physical and chemical properties. Soil Sci. 161 (1), 9–20.
Pronk, G.J., Heister, K., Kögel-Knabner, I., 2011. Iron oxides as major available interface component in loamy arable topsoils. Soil Sci. Soc. Am. J. 75 (6), 2158.
Puget, P., Chenu, C., Balesdent, J., 2000. Dynamics of soil organic matter associated with particle-size fractions of water-stable aggregates. Eur. J. Soil Sci. 51 (4), 595–605.
Quideau, S.A., Anderson, M.A., Graham, R.C., Chadwick, O.A., Trumbore, S.E., 2000. Soil organic matter processes: characterization by ^{13}C NMR and ^{14}C measurements. For. Ecol. Manag. 138 (1), 19–27.
Rasmussen, C., Heckman, K., Wieder, W.R., Keiluweit, M., Lawrence, C.R., Berhe, A.A., Blankinship, J.C., Crow, S.E., Druhan, J.L., Hicks Pries, C.E., Marin-Spiotta, E., Plante, A.F., Schädel, C., Schimel, J.P., Sierra, C.A., Thompson, A., Wagai, R., 2018. Beyond clay: towards an improved set of variables for predicting soil organic matter content. Biogeochemistry 137 (3), 297–306.
Schjønning, P., de Jonge, L.W., Munkholm, L.J., Moldrup, P., Christensen, B.T., Olesen, J.E., 2012. Clay dispersibility and soil friability—testing the soil clay-to-carbon saturation concept. Vadose Zone J. 11 (1), 0.
Schöning, I., Morgenroth, G., Kögel-Knabner, I., 2005. O/N-alkyl and alkyl C are stabilised in fine particle size fractions of forest soils. Biogeochemistry 73 (3), 475–497.
Schröder, P., Huber, B., Olazábal, U., Kämmerer, A., Munch, J.C., 2002. Land use and sustainability: FAM research network on agroecosystems. Geoderma 105 (3–4),

155–166.
Six, J., Callewaert, P., Lenders, S., De Gryz, S., Morris, S.J., Gregorich, E.G., Paul, E.A., Paustian, K., 2002a. Measuring and understanding carbon storage in afforested soils by physical fractionation. Soil Sci. Soc. Am. J. 66 (6), 1981–1987.
Six, J., Feller, C., Denef, K., Ogle, S.M., De Moraes Sa, J.C., Albrecht, A., 2002b. Soil organic matter, biota and aggregation in temperate and tropical soils - effects of no-tillage. Agronomie 22 (7–8), 755–775.
Sommer, M., Wehrhan, M., Zipprich, M., Weller, U., Zu Castell, W., Ehrich, S., Tandler, B., Selige, T., 2003. Hierarchical data fusion for mapping soil units at field scale. Geoderma 112 (3–4), 179–196.
Stewart, C.E., Paustian, K., Conant, R.T., Plante, A.F., Six, J., 2007. Soil carbon saturation: concept, evidence and evaluation. Biogeochemistry 86 (1), 19–31.
Stewart, C.E., Plante, A.F., Paustian, K., Conant, R.T., Six, J., 2008. Soil carbon saturation: linking concept and measurable carbon pools. Soil Sci. Soc. Am. J. 72 (2), 379–392.
Torn, M.S., Trumbore, S.E., Chadwick, O.A., Vitousek, P.M., Hendricks, D.M., 1997. Mineral control of soil organic carbon storage and turnover. Nature 389 (6647), 170–173.
Totsche, K.U., Amelung, W., Gerzabek, M.H., Guggenberger, G., Klumpp, E., Knief, C., Lehndorff, E., Mikutta, R., Peth, S., Prechtel, A., Ray, N., Kögel-Knabner, I., 2018. Microaggregates in soils. J. Plant Nutr. Soil Sci. 181, 104–136.
Virto, I., Barré, P., Chenu, C., 2008. Microaggregation and organic matter storage at the silt-size scale. Geoderma 146 (1), 326–335.
Virto, I., Moni, C., Swanston, C., Chenu, C., 2010. Turnover of intra- and extra-aggregate organic matter at the silt-size scale. Geoderma 156 (1–2), 1–10.
von Lützow, M., Kögel-Knabner, I., Ekschmitt, K., Flessa, H., Guggenberger, G., Matzner, E., Marschner, B., 2007. SOM fractionation methods: relevance to functional pools and to stabilization mechanisms. Soil Biol. Biochem. 39 (9), 2183–2207.
Wagner, S., Cattle, S.R., Scholten, T., 2007. Soil-aggregate formation as influenced by clay content and organic-matter amendment. J. Plant Nutr. Soil Sci. 170 (1), 173–180.
Webster, R., Lark, R.M., 2013. Nested sampling and analysis. In: Field Sampling for Environmental Science and Management. Routledge, London, UK.
Weller, U., Zipprich, M., Sommer, M., Castell, W.Z., Wehrhan, M., 2007. Mapping clay content across boundaries at the landscape scale with electromagnetic induction. Soil Sci. Soc. Am. J. 71 (6), 1740.
Wiesmeier, M., Urbanski, L., Hobley, E., Lang, B., von Lützow, M., Marin-Spiotta, E., van Wesemael, B., Rabot, E., Ließ, M., Garcia-Franco, N., Wollschläger, U., Vogel, H.J., Kögel-Knabner, I., 2019. Soil organic carbon storage as a key function of soils - a review of drivers and indicators at various scales. Geoderma 333, 149–162.
Wilding, L.P., 1985. Spatial variability: its documentation, accommodation, and implication to soil surveys. In: Nielsen, D.R., Bouma, J. (Eds.), Soil Spatial Variability. Pudoc, Wageningen, The Netherlands.
Yu, H., Ding, W., Chen, Z., Zhang, H., Luo, J., Bolan, N., 2015. Accumulation of organic C components in soil and aggregates. Sci. Rep. 5, 13804.